PHILOSOPHICAL TRANSACTIONS A

rsta.royalsocietypublishing.org

Research

Article submitted to journal

Subject Areas:

xxxxx, xxxxx, xxxx

Keywords:

xxxx, xxxx, xxxx

Author for correspondence:

Zoltan Dombovari

e-mail: dombovari@mm.bme.hu

Experimental Observations on Unsafe Zones in Milling Processes

Zoltan Dombovari[1,2], Alex Iglesias[2], Tamas G. Molnar[1], Giuseppe Habib[1], Jokin Munoa[2], Rachel Kuske[3] and Gabor Stepan[1]

[1]Budapest University of Technology and Economics, Department of Applied Mechanics, Muegyetem rkp. 3, H1111 Budapest, Hungary

[2]IK4-IDEKO Dynamics & Control Department, Arriaga Kalea 2, E20870 Elgoibar, Spain

[3]Georgia Institute of Technology, School of Mathematics, 686 Cherry St NW, GA30313 Atlanta, USA

The unsafe zone in machining is a region of the parameter space where steady-state cutting operations may switch to regenerative chatter for certain perturbations, and vica versa. In case of milling processes, this phenomenon is related to the existence of an unstable quasiperiodic oscillation, the in-sets of which limit the basin of attraction of the stable periodic motion that corresponds to the chatter-free cutting process. The mathematical model is a system of time-periodic nonlinear delay differential equations. It is studied by means of a nonlinear extension of the semidiscretization method, which enables the estimation of the parameter ranges where the unsafe (also called bistable) zones appear. The theoretical results are checked with thorough experimental work: first, step-by-step parameter variations are adapted to identify hysteresis loops, then harmonic burst excitations are used to estimate the extents of the unsafe zones. The hysteresis loops are accurately distinguished from the dynamic bifurcation phenomenon that is related to the dynamic effect of slowly varying parameters. The experimental results confirm the existence of the bistable parameter regions.

THE ROYAL SOCIETY PUBLISHING

1. Introduction

Milling processes (see figure 1*a*) are subjected to a so-called surface regeneration effect due to the rotating motion of the tool: one of the cutting edges leaves a pattern on the machined surface (see figure 2*a*), which is then cut by the subsequent cutting edge. This effect was recognized and modelled via delayed vibratory states by the pioneers of the field in the 1950's [1,2], while the mathematical theory of the governing delay differential equations (DDE's) was established later [3]. The phenomenon has been in the focus of many studies (for examples, see [4–8]) due to the practical relevance of avoiding chatter. Chatter is an undesired vibratory motion of the cutting tool relative to the machined workpiece; its sound is clearly distinguishable from that of a chatter-free cutting process. If the relatively low-frequency vibration modes of machine tool structures are involved in chatter then fatigue may damage the machines [9], while high-frequency chatter increases cutting edge wear [10] and reduces machined surface quality [11].

Due to the periodic cutter/workpiece engagement (CWE), the milling process is also subjected to both external forcing and parametric excitation, which have time-period that is identical to the tooth pass period, i.e., to the delay [12]. The corresponding time-periodic response of the system is actually the desired stationary (or steady-state) cutting process. The onset of chatter is related to the loss of stability of this desired periodic motion. Stability can be predicted by means of linearization around this stationary periodic motion, which leads to a non-trivial problem when both parametric excitation and time delay are present (see [13–16]). In practice, the results of these calculations are usually summarized and visualized in the so-called stability lobe diagrams (SLD's) [17] where the stability boundaries are depicted with respect to the two most relevant cutting parameters: the spindle speed Ω and the axial depth of cut a. Along the stability boundaries, two types of vibrations occur: the classical self-excited ones are related to generalized Hopf bifurcations (H), also called Neimark-Sacker bifurcations, while the period doubling vibrations occur at flip bifurcations, also called period doubling (PD) bifurcations [18].

If SLD's are calculated in manufacturing industry, the most commonly used method is the so-called zeroth order approximation (ZOA) [19], which is based on time averaging that neglects most of the effects of parametric excitation. This can be considered as a modified D-subdivision method [20], which uses directly the frequency response functions (FRF's) of the machine tool/tool/workpiece system. More accurate SLD's can be constructed by applying Floquet theory [13] to extend ZOA with further frequency modulations; these are often referred to as the multi-frequency (MF) solutions in the literature [16,21–24].

Accurate SLD's can also be produced with so-called time-domain based methods. These include weighted residual methods such as collocation techniques, different polynomial based methods and least square based solutions [25]. The most straightforward method is the semidiscretization method (SDM), which is based on the discretizetion of the delayed state only [26–29], while the time derivatives are kept without discretization. Most of the roughing operations can be accurately analysed by fast ZOA algorithms. However, especially for finishing operations that typically involve interrupted milling processes [30], MF or time domain based solutions are needed to describe mode interactions [31] and to identify all the stability boundaries with PD bifurcations [32].

The cutting force acting at the cutting edge is an essential part in the mathematical models of milling processes. Its dependence on the state variables is influenced by many underlying physical phenomena that are still unexplored in their full complexity. All these effects are combined in the so-called cutting force characteristics, which is still determined empirically by extensive laboratory tests [17]. It is typical to consider the cutting force proportional to the chip width w and as a function of the local chip thickness h described by a specific cutting force characteristics $\mathbf{f}(h)$. For this, there are several simplified mathematical expressions: linear (L), shifted linear (SL), power (P), cubic polynomial (C) and exponential (E) functions (see figure 1*c*, [33]). Note that many of these expressions involve nonlinearity, which has key importance

in what follows. Moreover, the cutting force is 'switched off' when the chip thickness becomes zero or 'negative'. This introduces also a kind of non-smooth behaviour [34] in the system.

In autonomous systems, Hopf bifurcation means that, at the stability boundary of the steady-state (trivial) solution, a periodic motion (limit cycle) emerges, which is stable or unstable around the unstable or stable steady state solution, then referred to as super- or subcritical Hopf bifurcations, respectively [35]. This applies directly for the autonomous models of turning processes. The theory was extended for time-periodic [13] and for delayed systems [3] using infinite dimensional state spaces. In time-periodic systems, the role of the trivial solution is taken by periodic ones, and the role of limit cycles are taken by quasi-periodic oscillations with two essential frequencies, one of them related to the time-periodicity of the system.

There are numerous studies on the 'criticality' (in other words, on the sense) of the bifurcations in manufacturing processes. Most of them report subcritical behaviour, which implies the 'unsafe' nature of the cutting processes as explained later in detail [30]. These calculations are analytically demanding: normal form theory can be combined with centre manifold reduction [36–40], alternatively, multiple scales [41] or Galerkin methods [42] can be applied. Numerical solutions are also available by solving the related boundary value problem and calculating the emerging invariant limit cycle in autonomous systems (like turning) or invariant torus in the time-periodic case (like milling) [33,40,43,44]. The subcriticality induces the coexistence of the stable stationary cutting (SSC) solution and the chattering solution in a bistable [45] or unsafe zone [46] in the SLD's close to the stability boundaries. Subcritical phenomena are usually identified experimentally by means of the so-called hysteresis measurement [46] (figure 2*d*), when one of the key cutting parameters (usually the chip width or the axial depth of cut) is selected as bifurcation parameter, and it is first increased and then decreased sweeping through the critical domain around the stability limit. The unstable object is assumed to exist between the separated stable branches of the hysteresis loop. There exist more advanced techniques to trace unstable periodic orbits experimentally by means of feedback [47], but this kind of control was not realizable due to the lack of appropriate actuators.

There is a critical point of this type of experiments: the slowly varied bifurcation parameter may slightly modify the bifurcation phenomenon, which is also called dynamic bifurcation effect [48]. This means that due to the continuous variation of the bifurcation parameter, the transition between the stable and unstable states occurs beyond the transition point for the constant parameters case. This shift can also be taken as hysteresis by mistake.

The goal of this study is to confirm the existence of the unsafe (bistable) zones in milling processes by means of extensive experimental work that excludes the effect of slowly variable parameters. In order to achieve this goal, the measurements have to be planned carefully by taking into account the theoretical linear and nonlinear behaviour of the regenerative phenomenon occurring in different milling operations (see figure 1*ad*).

(a) Review on surface regeneration

Surface regeneration is the most influential phenomenon that affects the milling process. Most of the chatter suppression techniques [49] are based on the disruption of simple regeneration of the one single constant delay τ in dynamic models. This delay is actually equal to the tooth passing period $T_Z = 2\pi/\Omega_Z = 2\pi/\Omega/Z$ for a conventional helical milling tool with Z number of equally spaced cutting teeth (figure 1*d i*).

To describe special milling tools one needs to model irregularly spaced pitch angles φ_{p}, irregular helix angle η, and the irregular local geometry described by the lead angle κ and the local radii R (see figure 1). Moreover, spindle speed can be modulated, too, that directly disturbs the regeneration in time. In order to describe the dynamics of milling, the angular position $\varphi_i(z,t)$ (figure 1*a*) of the cutting edge i currently in cut must be traced along the axial axis z of the tool. Besides, the corresponding angular position of the $(i+l)$th edge in the past $\varphi_{i+l}(z, t-\tau_{i,l}(z,t))$ that produced the surface underneath the ith edge must also be found. By assuming moderate feed v_f and vibration amplitude to the tool envelope diameter D, the following relationship

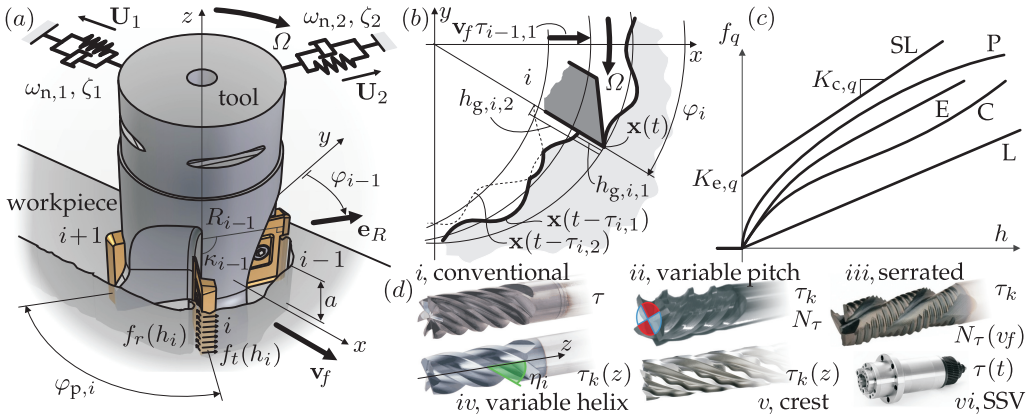

Figure 1: (a) shows the sketch of the milling operation. (b) shows the regeneration effect in milling with $h_{\mathrm{g},i} = \min_l h_{\mathrm{g},i,l}$ (1.2), while (c) shows the different cutting force characteristics ($q = t, r, a$) used in the literature [33]. Part (d) presents the different chatter suppression techniques [49] designed based on the disturbance of the simple delay τ of conventional ($d\,i$) milling tool.

holds: $\varphi_i(z,t) = \varphi_{i+l}(z, t - \tau_{i,l}(z,t))$. Without detailing the description [50,51], helix and pitch variation of the edges can be described by $\varphi_{\mathrm{p},i}(z)$ ($i = 1, 2, \ldots, Z$) functions. Since irregular radii $R_i(z)$ can cause missed cuts [50], while larger amplitude vibration can lead to fly-over [30], delays can occur in all possible consecutive combinations of the pitch angle functions. Thus, the following can be stated

$$\sum_{k=1}^{l-1} \varphi_{\mathrm{p},(i+k) \bmod Z}(z) = \int_{t-\tau_{i,l}(z,t)}^{t} \Omega(\xi)\mathrm{d}\xi, \tag{1.1}$$

which leads to an explicit formula for the delay if $\Omega(t) = \Omega$, but remains an implicit definition if $\Omega(t)$. To assess which delay is effective at the current cut, the minimum of all possible chip thickness values is taken as

$$\begin{aligned} h_{\mathrm{g},i}(z,t) \approx \min_l \big(\mathbf{n}^{\mathsf{T}}(\varphi_i(z,t),z) \big(\mathbf{x}(t) - \mathbf{x}(t-\tau_{i,l}(z,t)) + \tau_{i,l}(z,t)\mathbf{v}_f + \\ (R_i(z) - R_{i+l}(z))\mathbf{e}_R(\varphi_i(z,t))\big)\big), \end{aligned} \tag{1.2}$$

$$h_i(z,t,\mathbf{x}_t(\vartheta)) := g_{\mathrm{fo},i}(z,t) h_{\mathrm{g},i}(z,t), \quad g_{\mathrm{fo},i}(z,t) = H(h_{\mathrm{g},i}(z,t)), \tag{1.3}$$

according to [52] (see figure 1b). The so-called geometric chip thickness h_{g} in (1.2) is approximated as the projection of the local movement of the cutting edge to the local normal direction $\mathbf{n}$ [50]. In (1.2) $\mathbf{e}_x$ represents the feed direction, while $\mathbf{e}_R$ is the local radial direction perpendicular to z (see figure 1a). Since h_{g} can be negative, a screen function g_{fo} is introduced using the Heaviside step function H, which leads to the real effective chip thickness h in (1.3) [33].

In contrast to the conventional helical tool (figure 1$d\,i$) with a single constant delay $\tau_{i,l}(z,t) = \tau$, variable pitch tools (figure 1$d\,ii$) introduce up to $N_\tau \leq Z$ different constant delays $\tau_{i,l}(z,t) = \tau_k$ ($k = 1, 2, \ldots, N_\tau$). This kind of tools are available in the market, although their optimal selection is important to achieve the expected performance [53]. The so-called serrated cutters have varying local radii $R_i(z)$ that produce a spatial phase shift between the consecutive edges (figure 1$d\,iii$). This way, more disturbance in the regeneration can be introduced by intentionally creating missed cuts [50,54] with constant delays $\tau_{i,l}(z,t) = \tau_k$ ($N_\tau \leq Z^2 - (Z-1)$). Using the correct feed, these tools can approach the ideal 'one-tooth' good stability properties. Moreover, serrated tools utilize the degressive nature of the nonlinear cutting force characteristics (figure 1c) by setting the workpoint to a higher feed region [50]. Linear (figure 1$d\,iv$) and nonlinear (figure 1$d\,v$) variation on the helix introduces continuous variation of the pitch angles, thus, $\tau_{i,l}(z,t) = \tau_k(z)$ [55–59].

This continuous variation of the delay can be described mathematically with distributed delays [51]. These tools are also available in the market, while their performance and selection are still in question. Finally, spindle speed variation (figure 1*d vi*) introduces time dependency of the delay $\tau_{i,l}(z,t)$ as in (1.1) [60–62]. Special tools are important at the high spindle speeds, while spindle speed variation is effective in low spindle speed zones, especially for turning operation [49].

In this work we consider conventional tools with regular edge geometry subject to constant spindle speed $\Omega(t)=\Omega$, which results in a single constant delay $\tau_{i,l}(z,t)=\tau=T_Z$.

(b) Equations of motion

The general form obtained from experimental modal analysis [63] is given as

$$\dot{\mathbf{q}}(t)-[\lambda_l]_{l=1}^{2n}\,\mathbf{q}(t)=\mathbf{U}^{\mathsf{T}}\,\mathbf{F}(t,\mathbf{x}_t(\theta)), \tag{1.4}$$

where $\lambda_k=-\zeta_k\omega_{\mathrm{n},k}+\omega_{\mathrm{d},k}\mathrm{i}$ ($k=1,2,\ldots,n$ and $\lambda_{n+k}=\overline{\lambda}_k$). The kth damped natural angular frequency $\omega_{\mathrm{d},k}$ originates from the undamped one $\omega_{\mathrm{n},k}$ and the modal damping ratio ζ_k as $\omega_{\mathrm{d},k}=\omega_{\mathrm{n},k}\sqrt{1-\zeta_k^2}$. The mass normalized modal transformation matrix $\mathbf{U}$ contains $2n$ mode shapes $\mathbf{U}_k$. This transforms the modal coordinates $\mathbf{q}$ to spatial (x,y,z) ones as $\mathrm{col}(\mathbf{x},\dot{\mathbf{x}})=\mathrm{col}(\mathbf{U},\mathbf{U}[\lambda_l]_{l=1}^{2n})\mathbf{q}$.

The expression of the cutting force reads

$$\mathbf{F}(t,\mathbf{x}_t(\theta))=-\sum_{i=1}^{Z}\int_0^a g_{\mathrm{ri},i}(z,t)g_{\mathrm{fo},i}(z,t)\frac{\mathbf{T}_i(z,t)\,\mathbf{f}(h_i(z,t,\mathbf{x}_t(\theta)))}{\cos\eta_i(z)\,\sin\kappa_i(z)}\mathrm{d}z, \tag{1.5}$$

which is integrated over the axial depth of cut a (for more details, see [33]). $\mathbf{f}(h)$ indicates the empirical specific cutting force characteristics and it is defined after Endres [64] (E in figure 1*c*) in this work as

$$\mathbf{f}(h)=\mathrm{col}_j\,f_j(h)=\mathrm{col}_j\left(K_{\mathrm{c},j}h+K_{\mathrm{e},j}\left(1-\mathrm{e}^{-E_jh}\right)\right), \tag{1.6}$$

where $K_{\mathrm{e},j}$ are edge coefficients, $K_{\mathrm{c},j}$ are cutting coefficients (similarly to the well-known shifted linear characteristics, SL in figure 1*c*, whereas E_j are Endres' [64] exponential factors in the tangential t, radial r and axial a directions ($j=t,r,a$).

The main goal of this paper is to experimentally show the special bistable behaviour of milling processes based on the properties of a time-periodic $\mathbf{x}_{\mathrm{P}}(t;\Omega_Z)$ and a quasi-periodic $\mathbf{x}_{\mathrm{QP}}(t;\Omega_Z,\omega)$ solution of (1.4) considering conventional milling process with constant spindle speed, when $\mathbf{F}(t,\mathbf{x}_t(\theta))=\mathbf{F}(t,\mathbf{x}(t),\mathbf{x}(t-\tau))$ (1.5).

(c) Linear stability

In order to analyse stability, one can introduce a so-called variational equation [13] 'around' the period-one stationary solution $\mathrm{col}(\mathbf{x}_{\mathrm{P}},\dot{\mathbf{x}}_{\mathrm{P}})=\mathrm{col}(\mathbf{U},\mathbf{U}[\lambda_l]_{l=1}^{2n})\mathbf{q}_{\mathrm{P}}$ with time period $T_Z=\tau$

$$\dot{\mathbf{u}}(t)=\mathbf{D}(t)\mathbf{u}(t)+\mathbf{E}(t)\mathbf{u}(t-\tau)+\mathbf{g}(t,\mathbf{u}(t),\mathbf{u}(t-\tau)), \tag{1.7}$$

where $\mathbf{q}=\mathbf{q}_{\mathrm{P}}+\mathbf{u}$. The time-periodic coefficient matrices are

$$\mathbf{D}(t)=[\lambda_k]_k^{2n}+\mathbf{U}^{\mathsf{T}}\frac{\partial\mathbf{F}}{\partial\mathbf{x}(t)}(t,\mathbf{x}_{\mathrm{P}}(t),\mathbf{x}_{\mathrm{P}}(t))\mathbf{U},\quad \mathbf{E}(t)=\mathbf{U}^{\mathsf{T}}\frac{\partial\mathbf{F}}{\partial\mathbf{x}(t-\tau)}(t,\mathbf{x}_{\mathrm{P}}(t),\mathbf{x}_{\mathrm{P}}(t))\mathbf{U}, \tag{1.8}$$

respectively, while $\mathbf{g}(t,\bullet,\bullet)$ contains the higher order terms. Note that the stability of $\mathbf{x}_{\mathrm{P}}$ or, equivalently, the stability of the trivial solution of (1.7) is a general requirement for a good quality milling operation, where vibrations occur due to periodic forcing only. First, the linear part of (1.7) is considered for stability analysis. According to the Floquet theory [13], the stability of the

linear part of system (1.7) is determined by the monodromy operator $U(T)$

$$\mathbf{u}_T(\theta) = (U(T)\mathbf{u}_0)(\theta). \tag{1.9}$$

The spectrum of the linear operator $U(T)$ consists of so-called characteristic multipliers denoted by μ. If all multipliers lie inside the unit-circle of the complex plane, the time-periodic stationary solution is asymptotically stable.

There exist several semi-analytical methods to discretize the operator $U(T)$ and approximate it with a matrix $\mathbf{A}$ whose eigenvalues approximate the dominant characteristic multipliers (see [25]). These methods lead to the following form

$$\mathbf{z}_p = \mathbf{A}\mathbf{z}_0, \tag{1.10}$$

where $p \in \mathbb{N}$ is the resolution of the time period, $\mathbf{z}_j = \mathrm{col}_{l=0}^{r}\, \mathbf{u}_{t_j}(-l\Delta\theta)$ is the discretized state with $t_0 = 0$, $t_p = T$, $\Delta\theta = \Delta t = T/p$, and $r = \lfloor \tau/\Delta\theta \rfloor$ is the delay resolution. The semidiscretization method (SDM) [27] is one of the simplest among these methods, which serves sufficiently accurate results within reasonable computational time. In this paper, we used SDM to predict SLD's (see figure 3).

(d) Prediction of unstable tori

A nonlinear extension of the SDM [65] allows one to compute an approximation of the unstable invariant quasi-periodic torus that arises from the stability boundary associated with Hopf bifurcation. Via semidiscretization of the nonlinear system (1.7), a nonlinear map can be constructed that approximates the nonlinear dynamics over the principal period T_Z. A third-order approximation of this map can be given in the form

$$\mathbf{z}_p = \mathbf{A}\mathbf{z}_0 + \frac{1}{2}\langle \mathbf{B}, \mathbf{z}_0, \mathbf{z}_0 \rangle + \frac{1}{6}\langle \mathbf{C}, \mathbf{z}_0, \mathbf{z}_0, \mathbf{z}_0 \rangle\,, \tag{1.11}$$

where $\mathbf{A}$ is the coefficient matrix of the linear term, cf. (1.10), while $\mathbf{B}$ and $\mathbf{C}$ are the third- and fourth-order coefficient matrices of the quadratic and cubic terms. These matrices can be obtained from $\mathbf{D}$, $\mathbf{E}$ and $\mathbf{g}$ in (1.7) by using the formulas in [65]. The products denoted by angle brackets are defined as $\langle \mathbf{B}, \mathbf{x}, \mathbf{y} \rangle := [B_{jkl} x_k y_l]$, $\langle \mathbf{C}, \mathbf{x}, \mathbf{y}, \mathbf{z} \rangle := [C_{jklm} x_k y_l z_m]$ using index notation.

Via bifurcation analysis of the trivial fixed point of map (1.11) [66], the occurrence of invariant tori can be predicted and their unstable behaviour can be shown. A constant parameter δ_{cr} can be computed from the coefficient matrices in (1.11), whose sign determines the stability of the arising invariant tori (they are unstable for $\delta_{\mathrm{cr}} > 0$ and stable for $\delta_{\mathrm{cr}} < 0$). In addition, the approximate amplitude r of the solutions located on the invariant tori can be calculated according to [67]

$$r(a) \approx \sqrt{-\frac{|\mu|'_{\mathrm{cr}}(a - a_{\mathrm{cr}})}{\delta_{\mathrm{cr}}} \frac{a_{\mathrm{cr}}}{a}}\,. \tag{1.12}$$

Here, a_{cr} is the critical axial depth of cut at the boundary of stability and $|\mu|'_{\mathrm{cr}}$ is the so-called root tendency, which is associated with the eigenvalues of matrix $\mathbf{A}$ (for details, see [65]). Note that this expression excludes the existence of invariant tori for zero axial depth of cut ($a = 0$), where (1.4) simplifies to a damped free oscillator that has no periodic or quasi-periodic solutions [67].

The results help to quantify the extent of the bistable zones in the space of technological parameters. The comparison of the experimental and theoretical bifurcation diagrams also helps select a simple but still accurate enough nonlinear cutting force characteristics $\mathbf{f}(h)$ that satisfy the requirements of manufacturing industry.

2. Revealing unsafe zone in milling processes

In this section, different measurement techniques capturing the unsafe zone phenomenon in milling processes are summarized. Special attention is paid to the existence and sensitivity of this phenomenon. While its existence can be investigated relatively easily (for example with a harsh

entrance into the workpiece, see figure 2*ab*, an exact quantitative description of its sensitivity is an extremely complicated task.

To establish an effective measurement technique for the experimental investigation of the unsafe zone, one needs to distinguish between stable stationary cutting (SSC) and stable chattering (limiting) motion (CH). These can exist simultaneously for the same set of technological parameters, that is, mathematically speaking, bistability can occur. Although much larger amplitude is expected for chatter than for the stationary cutting state, this property cannot always be used for the direct detection of chatter. In measurement circumstances it may be impossible to measure oscillations directly at the tool tip and sensors must be further away from the cutting zone. In such cases, chatter may be detected by the inspection of its distinctive spectrum and/or the surface pattern left on the workpiece.

As it was shown in [68], an impact can induce a transition from stationary cutting process to chattering motion. This phenomenon is also shown in figure 2*c*, where a prepared laboratory experiment was used to demonstrate the existence of the unsafe zone. Although this hitting methodology appears simple and promising, the quantification of the perturbation caused by the impact is not trivial. Since the impulse is scattered all over the bandwidth, it might result in an unsatisfactory excitation around the sensitive (chatter) frequency. In addition, one might hit the process in the 'wrong direction' that does not induce chatter. Since the phase space of a DDE is infinite-dimensional, the perturbation may completely bypass the unstable invariant torus that repels the motion towards the chattering state [33].

One possible solution to avoid the quantification issues is the exploitation of hysteresis effects caused by the subcritical behaviour of cutting, which is a common approach in nonlinear dynamics. In milling, this can be realized by using a symmetric roof-shaped workpiece, by which a regular increase and decrease of the axial depth of cut is ensured (see figure 2*d*, [46]). Although the existence of the bistability phenomenon is clearly revealed by this method, the quantification of the bistable region leads to difficulties again. The slope of the roof-shaped workpiece must be small in order to improve measurement quality, since the theoretical prediction is typically performed by assuming constant bifurcation parameter in time. This assumption does not hold, since the finite (small) length of the workpiece results in a relatively steep and highly tilted upper surface causing significant rate of change in the axial depth of cut. Variation of the bifurcation parameter in time generates a dynamic bifurcation effect [48,69], which shifts even the linear stability boundaries depending on the sign and the rate of the parameter change. This shift may appear to be hysteresis while the real mechanisms behind bistability remain hidden.

To avoid the dynamic bifurcation effect, one can manufacture steps (figure 4*b*) on top of the workpiece. The steps result in a discrete increase and decrease of the axial depth of cut. However, due to the limited number of the steps that can be machined within the finite length of the workpiece, the resolution of this method is insufficient to determine the size of the unsafe zone accurately. This experimental method is suitable only for showing the existence of the unsafe zone phenomenon without involving a dynamic change of the bifurcation parameter, and for providing a rough estimation of the size of the unsafe zone. In the paper, this methodology is referred to as 'step measurement' (SM).

As a final approach, the idea of harmonic excitation is considered. The vibratory system is excited by a burst harmonic perturbation that mimics the chatter frequency. This experimental method needs sophisticated instrumentation. It requires a built-in actuator that is capable of providing the force needed to move the machine tool structure with a given amplitude and frequency. This was realized by a built-in inertial drive (ID) in a large heavy-duty milling machine as shown in figure 5*f*. This measurement technique is referred to as 'harmonic test' (HT).

This paper focuses on the dynamics of the SM and HT methodologies, in order demonstrate the existence of the unsafe zone, and to quantify the effect of unstable invariant tori without any effects from dynamic bifurcations. The conclusions use experimental observations that are then related to the analysis of a mechanical model of the milling process.

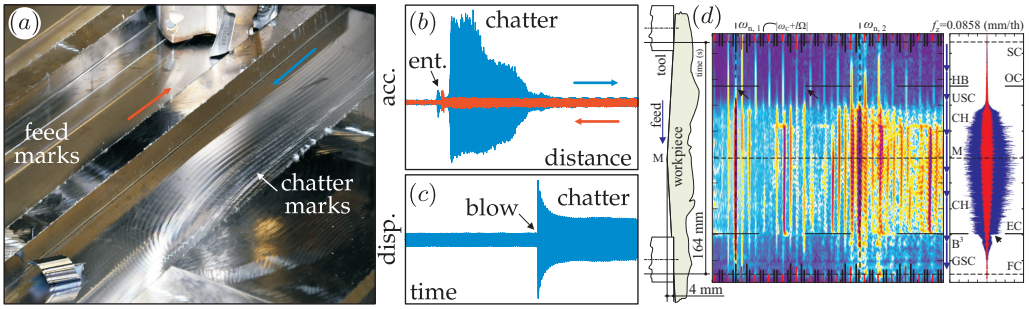

Figure 2: The effect of harsh workpiece entry (ent.) is presented in (ab). Bistability is triggered by a hammer blow similarly [68,70] in (c), while the rooftop measurement is presented in (d) [46].

3. Preliminary experiments

In order to conduct a series of measurements demonstrating the effect of unsafe zone, preliminary tests must be performed to characterize the workpiece material and the dynamic behaviour of the machine tool. In this section, cutting force characteristics, machine tool dynamics and linear stability are investigated experimentally and summarized for both the SM and HT cases. Note that the SM was performed in a laboratory while the HT took place in industrial environment.

A series of down milling (DM) tests were carried out for different chip thickness values using workpiece materials AL2024-T351 in SM and C45 in HT. For AL2024-T351, the nonlinear cutting force parameters in (1.6) were directly identified from a dense equidistant measurement set [17] resulting in: $K_{\mathrm{c},j} = (1049.8,\, 532.9,\, 0)\,\mathrm{MPa}$, $K_{\mathrm{e},j} = (13.4,\, 15.2,\, 0)\,\mathrm{kN/m}$ and $E_j = (66.9,\, 45.4,\, 0)\cdot 10^3/\mathrm{m}$. In the case of C45, the linear cutting force parameters $K_{\mathrm{e},j}$ and $K_{\mathrm{c},j}$ were measured only, since there was no possibility to perform extensive measurement series in the industrial environment of the HT: $K_{\mathrm{c},j} = (1889,\, 734,\, 387)\,\mathrm{MPa}$, $K_{\mathrm{e},j} = (69.7,\, 83.2,\, 87.6)\,\mathrm{kN/m}$. The exponents $E_j = 200\cdot 10^3/\mathrm{m}$ in the HT case were fit heuristically such that they do not contradict with the linear stability observations discussed below. Its value needs to be large enough to mimic the industrial shifted linear characteristics around the average chip thickness and small enough to capture finite tangent when the chip thickness vanishes.

Modal tap tests were also performed on the milling tool-tip to determine the overall dynamic behaviour of the milling machine (black lines in figure 3adg). The modal parameters were determined by assuming linear non-proportionally damped dynamics (red lines in figure 3adg [63,71]). The parameters were later used for linear stability analysis (see figure 3cfj). A smaller dominant set of proportional modes (blue lines and tables in figure 3, where $\mathbf{U}_k = \mathbf{p}_k/\sqrt{m_k}$ and $\|\mathbf{p}\| = 1$) were also used later for performing nonlinear SDM.

Experimental stability (chatter) tests were performed for both the SM and the HT in order to see the discrepancies from theoretical linear stability predictions. The results are summarized in figure 3. In the lab environment (SM), chatter tests were performed with machining properties MP$_1$:$\{Z = 2,\, a_{\mathrm{e}} = 10\,\mathrm{mm},$ DM, $D = 16\,\mathrm{mm},\, \kappa = 90\,\mathrm{deg},\, \eta = 30\,\mathrm{deg}\}$ (figure 3) on a dense grid of technological parameters, see the green circles (stable stationary cutting, SSC), the red crosses (chatter, CH) and the blue diamonds (undetermined case) in figure 3a. It is important to note that there is a difference from the theoretical prediction (black line) both in terms of elevation (axial depth of cut) and 'resonances' (natural frequencies). Both can be explained by the change of the dynamics during cutting compared to the non-operating (tap tested) case. In fact, for the SM setup a dummy tool was shot by softball and measured by laser displacement sensor in order to estimate varying dynamics during spindle rotation (without cutting). Modifying functions were used for $\omega_{\mathrm{n},k}(n)$ and $\zeta_k(n)$ accordingly [53] (figure 3c).

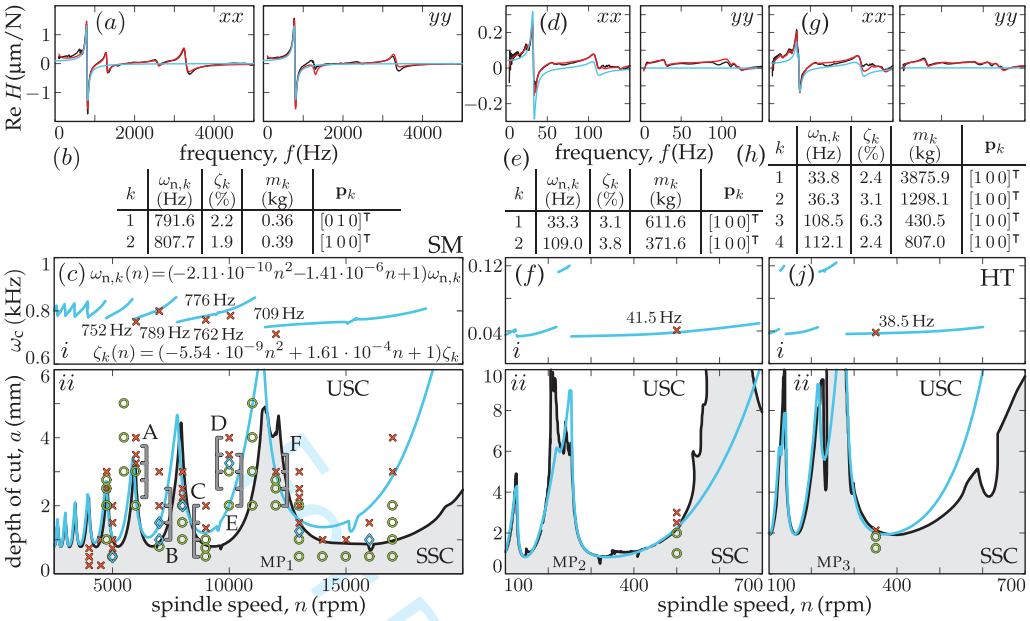

k	$\omega_{n,k}$ (Hz)	ζ_k (%)	m_k (kg)	$\mathbf{p}_k$
1	791.6	2.2	0.36	$[0\,1\,0]^T$
2	807.7	1.9	0.39	$[1\,0\,0]^T$

k	$\omega_{n,k}$ (Hz)	ζ_k (%)	m_k (kg)	$\mathbf{p}_k$
1	33.3	3.1	611.6	$[1\,0\,0]^T$
2	109.0	3.8	371.6	$[1\,0\,0]^T$

k	$\omega_{n,k}$ (Hz)	ζ_k (%)	m_k (kg)	$\mathbf{p}_k$
1	33.8	2.4	3875.9	$[1\,0\,0]^T$
2	36.3	3.1	1298.1	$[1\,0\,0]^T$
3	108.5	6.3	430.5	$[1\,0\,0]^T$
4	112.1	2.4	807.0	$[1\,0\,0]^T$

Figure 3: The left and right panels show results for SM and HT cases. The corresponding FRF's are shown in (adg), where black and red colours indicate the measured and the fit FRF's. Low-DOF proportional fit (beh) used for the nonlinear analysis is depicted by blue curves in (adg). Measured and calculated SLD's are shown for the lab SM (c) and industrial HT (fj) tests. For all MP's vibration (chatter) frequency plots i and the actual stability charts are presented ii. In ii black and blue curves are the non-proportional and the selected dominant proportional results boundaries. Stable and unstable stationary cutting (SSC/USC) tests are denoted by • and ×. Undetermined tests are denoted by ⋄.

In the industrial (HT) case, up milling (UM) chatter tests were performed at a chosen spindle speed only, in order to provide validation of theoretical stability analysis for each ram position. The samples corresponding to MP$_2$:{$Z=8$, $a_e=100$ mm, UM, $D=125$ mm, $\kappa=45$ deg, $\eta=0$ deg} and MP$_3$:{$Z=8$, $a_e=60$ mm, UM, $D=125$ mm, $\kappa=45$ deg, $\eta=0$ deg} are presented in figure 3fj, where some differences from theoretical results (shown by black and blue lines) were again experienced.

After the chatter tests, the nonlinear experiments were prepared based on the measured SLD's. In the SM case, spindle speeds are selected from the regions where the predicted and measured stability limits are close to each other. For the HT cases, the two validated spindle speeds are accepted for later nonlinear analysis.

4. Step measurement (SM)

The SM is one of the simplest approach to demonstrate the phenomenon of bistability while excluding the dynamic bifurcation effect. Based on the results of experimental chatter tests (figure 3c), the workpiece is prepared such that steps are machined onto it in increasing and then in decreasing order (figure 4b). Since the length of the workpiece is given, a trade-off must be made between the number and the length of steps. It is important at all steps to provide enough space (time) for the tool to reach its stationary state. Obviously, there is smaller possibility to capture the phenomenon of bistability in the SM than in the HT due to the limited resolution of axial depth of cut steps on the workpiece. When the measurements do not capture bistability, the

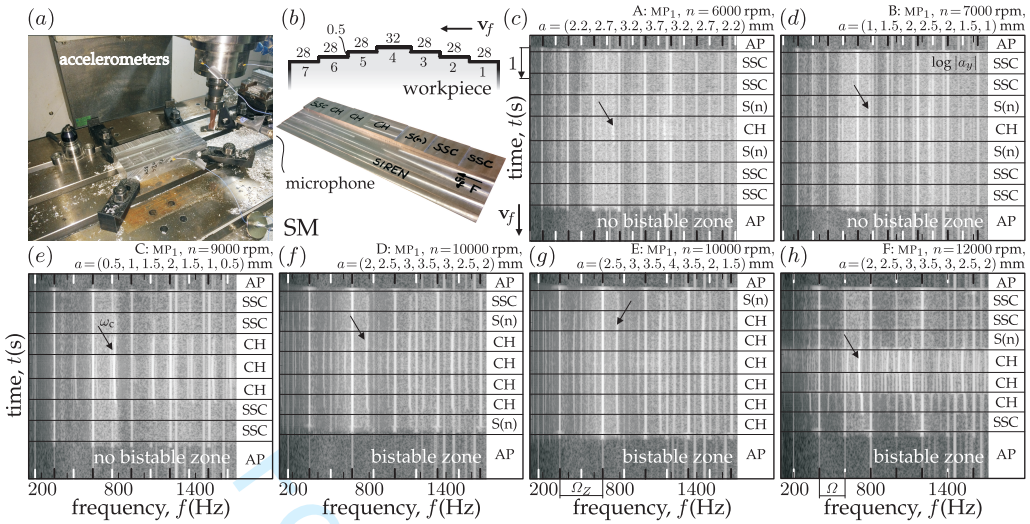

Figure 4: Summary of the step measurement SM performed with the first set of machining properties MP_1, whose setup is presented in panel (a). The geometry of the workpiece is presented in (b). The time-frequency diagram of the performed measurements A-F are presented in (c-h). The harmonics of the spindle and tooth passing frequencies are indicated by side ticks, while the dominant (chatter) frequency is marked by arrows. Bistable zones are demonstrated with asymmetric orders of the SSC: 'stable stationary cutting', CH: 'chatter', S(n): 'stable with noise resonance' cases. AP stands for 'approaching phases'. (see video footage [73].)

test results cannot be distinguished from supposingly linear chatter tests where instability should arise in symmetric arrangement along the steps.

For the measurements, we also use the industrial jargon to label vibration states as 'stable' as stable stationary cutting and 'chatter' (denoted by SSC and CH, respectively). In fact, all these states are related to a stable invariant object of the dynamical system (1.4). Chatter CH state involves both the evolved threshold vibration and the onset of amplifying vibrations originated, on the one hand, from the unstable stationary cutting (USC) period one solution $\mathbf{x}_P$. The stability loss is caused by an orbital Hopf bifurcation [13], which introduces dominant (chatter) frequency (figure 3 i) and its modulations [72]. The Hopf bifurcation in the nonlinear milling model is subcritical and gives rise to an unstable invariant torus branch (ITB) of quasi-periodic solutions $\mathbf{x}_{QP}$ with Ω_Z and ω_c. The arising subcritical branches can be found by e.g. nonlinear SDM [65] or path-following methods based e.g. collocation [33]. On the other hand, this unstable torus can also repel the process from the expected SSC to an amplifying solution toward the the threshold (CH) state that we hear and measure in the long term. The threshold vibration state can be quasi-periodic or chaotic resembling the frequency content of the linear solution [74]. Large amplitude severe chatter is typically more chaotic in nature and deviates more from the linear spectrum.

It is important to note that cutting is not a 'clean' process; specifically, for parameter values near the linear stability boundary, noise-induced coherence resonance activates oscillations with frequency content similar to that of chatter [75]. We denote this weak frequency content as S(n), which appears in the otherwise stable region. We distinguish between this coherence resonance and the threshold state of chatter using a heuristic approach based on the higher frequency modulation of the dominant chatter frequency ω_c (see A in figure 4c).

The results of the SM's are discussed below. The SM's that show an asymmetric pattern of SSC/S(n) and CH states indicates the existence of the bistable zone. Experiments with a symmetric pattern could either imply linear behaviour or indicate that the resolution of the steps was insufficient to reveal the asymmetry. Since we experienced not only symmetric but asymmetric

patterns, too, we believe the second is true. The performed SM's (A-F) are depicted in figure 4*c*-*h*. The corresponding axial depth of cut values span through the experimental stability limit shown by 'combs' in figure 3*c ii*. In all tests, the feed was $f_Z = 0.1$ mm/tooth, that is, the tool was rotating roughly 150 times at each step. Lateral acceleration signals were acquired in two directions on the spindle and in one on the workpiece, while sound pressure was also measured (figure 4*a*).

Wavelet transformation was performed for all signals to obtain a good quality time-frequency diagram. Among all recorded signals, the y-directional acceleration of the spindle carried the richest frequency spectrum (figure 4). In all time-frequency plots, harmonics of Ω and Ω_Z are indicated by white and black side-ticks. The instances where the axial depth of cut changed are indicated with thin 'horizontal' black lines. The dominant vibration (chatter) frequency is indicated by black arrow. Note that frequency contents, which do not have a relation with the actual cutting process can be identified at the approaching phase (AP) parts. According to figure 4, all measurements start with a defined SSC or S(n) state. Only three measurements (D, E, F) exhibit the bistability phenomenon, while the others are symmetric (measurements A, B, C).

In the symmetric case A, strong harmonics of $\Omega_Z = 200$ Hz appear, while harmonics of $\Omega = 100$ Hz are also visible due to tool run-out. Weak noise-induced coherence resonance appears in the critical dominant frequencies before and after the CH, identified as S(n). Measurement A & B contains brief but strong CH state in the middle of the tool path with weak modulations of slightly changing frequency. Clear chatter regions with strong base and modulation frequencies are arranged symmetrically in measurement C, where strong changes of the chatter frequencies can be followed. Measurement D starts with an SSC, followed by coherence resonance S(n) of the frequency associated with the critical eigenvalue, then transitioning to clear chatter case, which later appears as an asymmetric measurement case with strong chatter followed by S(n) in the end. This asymmetric arrangement is forming an evidence for bistability. The next measurement E starts in the coherence resonance state S(n), transitioning to strong asymmetric chatter till the end of the workpiece. Obviously, some doubt can appear in this case since the whole measurement started with an almost unstable case, but the chatter stays so strong in the end, without any sign of settle, we identified this case as a weak evidence for the bistability. Measurement F is the most clear proof of bistability; it illustrates a slight noise in the increasing depth cut part and strong chatter in the decreasing depth of cut part. Even if one considers the noisy S(n) state as CH (which is not the case), the following CH states still strongly support the existence of bistability.

The HT experiment was designed to overcome the resolution problems of the SM and to show that bistable zones can appear even for a large industrial machine with a different workpiece material.

5. Burst harmonic perturbation (HT)

This form of excitation can be considered as the controlled version of the hammer blow figure 2*c*, where the aim is to push the system out from its local SSC state by some form of disturbance. Note that HT avoids the potential confusion of the dynamic bifurcation effect, as shown in figure 2*d*. Here, according to the initial linear calculations presented in figure 3, we excite the system with a burst of harmonic force set to the calculated dominant vibration (chatter) frequency figure 3*i*. By gradually increasing the excitation amplitude of the built in exciter, theoretically the unstable object that separates the bistability can be found. It is important to emphasize that the exciter (inertial drive, ID) is mounted on the ram (see figure 5*f*), which means the excitation is really unlocalized. Without any characterization of the ID and the ram structural mechanics the real actual amplitude of the tool can not be given.

In this manner, the only aim is to show that there is a limit excitation amplitude that separates the SSC from CH. By avoiding any characterization of the ID this limiting value is a voltage value, which refers to the driving voltage amplitude of the injected harmonic excitation. A new vibratory state is introduced referred to this excitation burst denoted by E. During the E part the system is forced both by the cutting and the excitation forces resulting in a quasiperiodic forced state. It is

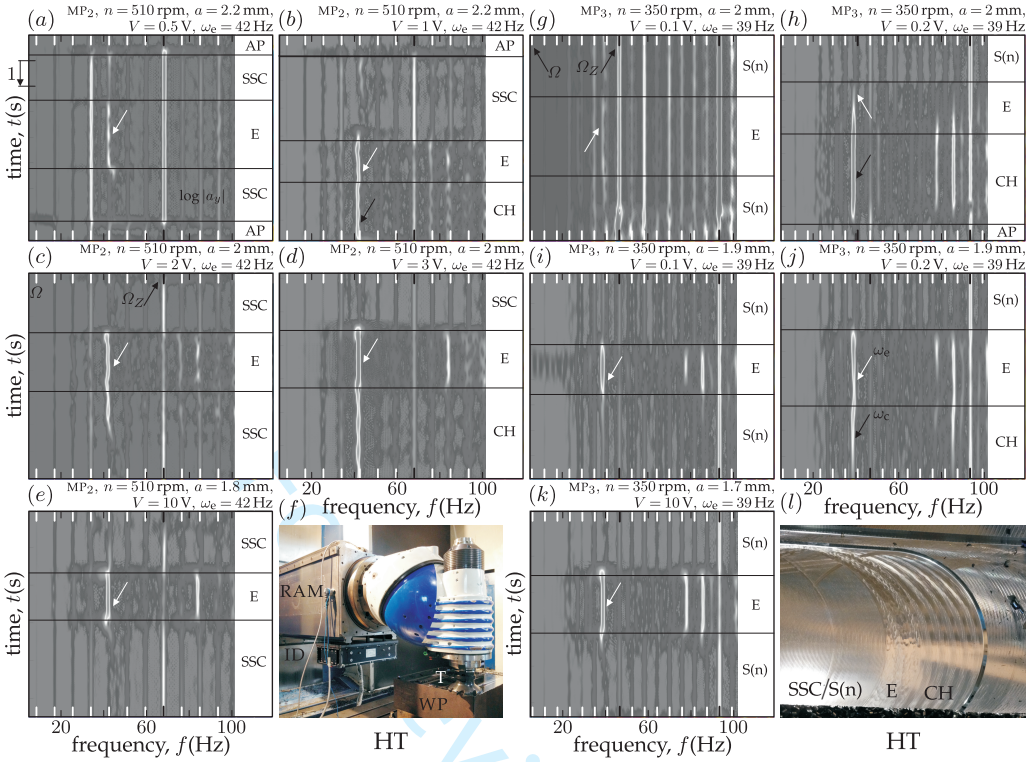

Figure 5: Panels (*a*-*e*) measurements are presented related to the second set of machining properties MP$_2$ with $n = 510$ rpm. In (*f*) the measurement setup is presented with a ram-type three axis heavy-duty milling machine on which an inertial drive ID was mounted. Panels (*g*-*k*) presents the results related to MP$_3$ with $n = 350$ rpm. In (*l*) a typical surface pattern is presented during SSC/E/CH cases. The different segments are indicated with 'horizontal' lines. The E state related to the external excitation is denoted by ID.

believed that this quasiperiodic forced state can push out the system to its threshold CH state and staying on after strictly ending the E part.

Due to the flexibility of the ram, the motion is also copied to the face surface of the workpiece, in which the different zones can be identified (figure 5*l*). The SSC creates the usual 'feed pattern', which is considered as the desired milling process. When the excitation switched on the system responses with a quasi-periodic forced state E. Then, by the vanishing external forcing from ID, the mechanical system has its 'free motion' (only excited by the regenerative cutting force) and the threshold motion CH might arise.

In this section, two measurement sets are presented related to the initial linear calculations (figure 3*fj*) for two different ram extensions. Among the measurement sets one of them can be considered as a clear evidence of bistability (HT, MP$_2$, figure 3*f*, figure 5*a*-*e*), while the other one (HT, MP$_3$, figure 3*j*, figure 5*g*-*k*) can be considered as a weak but valid proof.

As an initial measurement HT sets were performed at $\Omega = 500$ rpm, however the bistable effect was weak and except some successful trials the 500rpm was considered as a failed attempt. Then, the spindle speed was set to $\Omega = 510$ rpm, where it was possible to see and measure the phenomenon. The results presented in figure 5 are ordered from the top to the bottom with decreasing axial depth of cut a. The cutting process was completely CH at $a = 2.3$ mm. The first presented result at the top are for $a = 2.2$ mm, where the asymmetric (SSC/E/CH) behaviour can be realized for drive voltage amplitude $V = 1$ V (figure 5*b*), which vanishes at $V = 0.5$ V

(figure 5*a*). The spindle and tooth passing harmonics are denoted in the same manner as it was explained in Sec. 4. This measurement was considered as a successful strong evidence of bistability, even though using $V = 1\,\mathrm{V}$ (figure 5*b*) initially some self-excitation had appeared due to the entrance, which died out (figure 2*ab*). By decreasing the axial depth of cut to $a = 2\,\mathrm{mm}$ the limit voltage increased between $V = 2\,\mathrm{V}$ (figure 5*c*) and $V = 3\,\mathrm{V}$ (figure 5*d*). In this case the $V = 3\,\mathrm{V}$ case is strongly bistable, while in the case of $V = 2\,\mathrm{V}$ some leftover vibration remained after E part, but it died out. During the experiment, it was verified that a further decrease in the voltage would result in a more rapid 'die-out' of this leftover vibration, consequently it has considered as the limit for the selected a. In the last case, when $a = 1.8\,\mathrm{mm}$ no bistability was found (SSC/E/SSC) even using $V = 10\,\mathrm{V}$ (figure 5*e*) drive voltage amplitude for the inertial drive. According to this result, it can be concluded that the $\Omega = 510\,\mathrm{rpm}$ measurement shows the effect of subcritical Hopf bifurcation, namely, the appearance of the bistabile state 'below' the stability limit in a.

The next set of measurement was performed with lower ram extension for $\Omega = 350\,\mathrm{rpm}$ with MP_3. Again, the panels are ordered in a decreasing axial depth of cut manner from the top to the bottom in figure 5*g*-*k*. This set of measurement was more sensitive for perturbation and most of the cases the predicted dominant chatter frequency was a bit apparent in the time signals, even though it does not leave any recognizable mark on the surface (figure 5*l*). Notwithstanding, there was significant difference between the apparent chatter frequency and the really chattering case, distinguished with S(n) and CH. First, completely unstable (CH/E/CH, not presented here) case was measured at $a = 2.1\,\mathrm{mm}$. Then S(n)/E/S(n) and S(n)/E/CH types were experienced introducing $V = 0.1\,\mathrm{V}$ (figure 5*g*) and $V = 0.2\,\mathrm{V}$ (figure 5*h*) voltages, respectively, for $a = 2.0\,\mathrm{mm}$. By decreasing the depth of cut to first $a = 1.9\,\mathrm{mm}$, then to $a = 1.8\,\mathrm{mm}$ the limit voltage remained between $V = 0.1\,\mathrm{V}$ (figure 5*i*) and $V = 0.2\,\mathrm{V}$ (figure 5*j*). The weak bistability was demonstrated, although dominant (chatter) frequency was apparent during all tests, somewhat as a sign the operation was extremely close to the stability boundary. In the end at $a = 1.7\,\mathrm{mm}$ the system remained clearly stable (SSC/E/SSC) even setting $V = 10\,\mathrm{V}$ drive amplitude, as presented in figure 5*k*.

According to the result presented in this section the existence of the bistability is clearly demonstrated, although it was not apparent clearly in every trial. It can be considered as a quite remarkable achievement to experience this highly nonlinear phenomenon in this industrial case. Also, the difference in a does not seem significant, however, it reaches 10%, which can be considered as a small but noticeable difference.

6. Reconstruction of bifurcation diagrams

In this section, we construct the empirical bifurcation diagrams and compare them to the theory. In all examples, the transmissibility between the sensor locations and the tool tip was measured by using experimental modal analysis [63] to overcome the unlocalized nature of the signal acquisition (figure 4*a* & 5*f*). The stationary period one solution (SSC/USC) was predicted numerically, while the subcritical invariant torus branches (ITB's, [33]) were estimated by using nonlinear SDM (subsection 1.12) and path-following collocation method [33].

The comparison is presented in figure 6 both for the SM and HT cases. The bifurcation diagrams are constructed by adding the vibration amplitudes A_{st} and A_{c} corresponding to the tooth passing frequency Ω_Z of the stationary solution (forced vibration) and to the dominant chatter frequency ω_{c}, respectively, for various depths of cut a. In all cases presented in figure 6, the deviation between theoretical and experimental results can be attributed, on the one hand, to the significant discrepancies in linear stability predictions (figure 3*a ii*). This causes a shift in the diagrams with respect to a. On the other hand, there is a shift in the amplitude of the stationary solution (SSC/USC), too. This is due to the experienced runout of the two-fluted carbide milling tool, which affects the tooth passing harmonics Ω_Z by transferring kinetic energy to the spindle harmonics Ω. In figure 6 'hand'-fit experimental branches are depicted with thick lines, in which a similar trend can be recognized as in the theoretical predictions (thin lines). For example, it

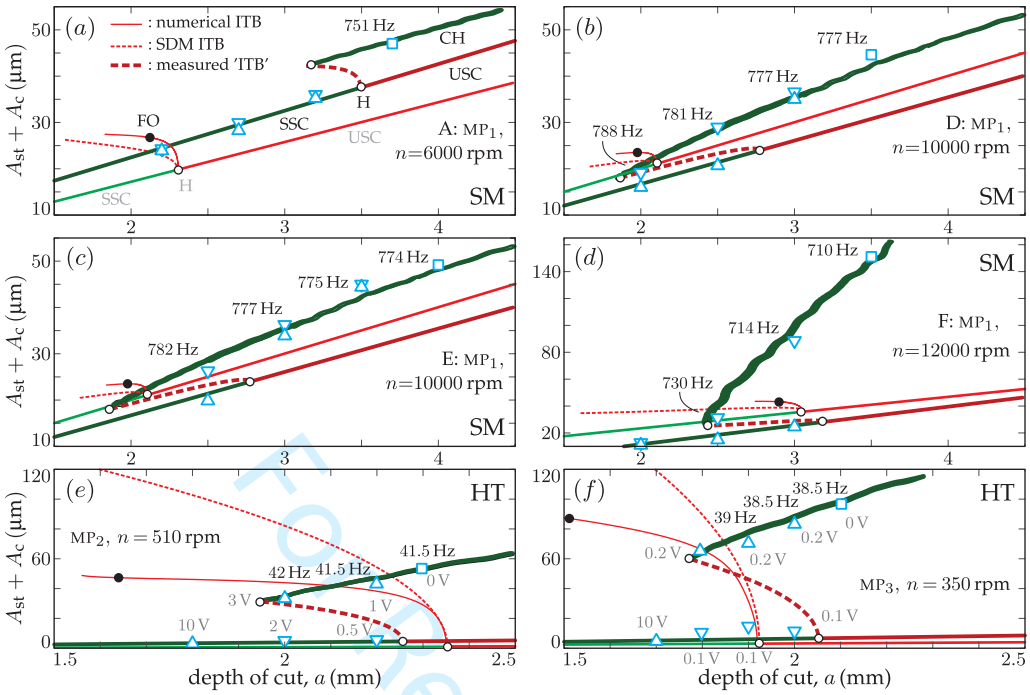

Figure 6: Comparison between the experimental and theoretical bifurcation diagrams. Both SM and HT cases are affected by the shift of the linear behaviour (see figure 3). In the diagrams, thin lines present the theoretical solutions, while thick ones represent the measurement results. Green and red correspond to stable and unstable objects, respectively. In SM case, △ and ▽ indicate increasing and decreasing step phases, while in HT, they indicate the measured amplitudes above and below the critical limit. Measurements □ correspond to measured CH states 'above' USC. Fly over points (FO) were determined according to [33] for the predicted diagrams.

can be explained why measurement A shows symmetric and why measurement F shows highly asymmetric arrangements in terms of a in figure 4. This is caused by the relative steepness of the quasiperiodic branch in figure 6 [33].

A much better correlation of theory and experiments can be observed in the HT (figure 6ef) case, where both bifurcation diagrams are better justified in terms of the Hopf point (H) and the vibration amplitudes. Note that only the measurement at $n = 510$ rpm in figure 6e can be considered as a clean test, due to the continuous slight appearance of the chatter frequency in the case $n = 350$ rpm presented in figure 6f. Regardless of the expected discrepancies in the stability limit (H), the curvature of the emerging unstable quasiperiodic branch (ITB) is well given by the theory, which results in lower vibration amplitude for the large amplitude chatter branch.

In all cases significant difference can be recognized between the invariant torus branches (ITB) constructed by nonlinear SDM and the path-following technique. This is due to the low order approximation of the SDM, which cannot follow the real curvature of the emerging ITB branches.

The first fly over moment (FO) can be realized by determining the local chip thicknesses (1.2). Theoretically this would refer to the size of the unsafe zone, but in milling this connection is questionable due to the multiple edges participating in the cutting process. Even by the consideration of minimum possible chip thickness [76], in SM cases, the FO point comes 'early' after the Hopf (H) point, which can cause the fold of these branches, rather experiencing supercritical nature right after the subcritical emerging. This would be opposite to the experienced really strong subcritical nature of e.g. test F in figure 4. In the HT cases the FO appears much

'further' from H points, due to the quite stiff y directional modes, which prevents 'early' fly over in the process. Moreover, due to the high edge number ($Z = 8$) the fold would appear after much more significant subcritical behaviour as it was experienced in the tests.

7. Conclusion

Milling processes in metal cutting are modelled by delay differential equations with parametric and external excitation. The desired cutting process corresponds to a stable periodic solution of these equations. When this periodic motion loses stability, undesired chatter occurs. Unfortunately, chatter may appear also due to large enough perturbations in parameter domains where the desired cutting process is stable. The existence of these so-called unsafe (or bistable) parameter domains has been shown theoretically and experimentally.

The bifurcation analysis of the periodic delay differential equation models predicted the existence of unstable quasi-periodic solutions emerging from a subcritical generalized Hopf (or Neimark-Sacker) bifurcation of the desired periodic solution. The nonlinear extension of the semidiscretization and the path-following collocation methods made it possible to carry out these calculations. The parameter points where the fly over effect appears first on the unstable quasi-periodic solutions were also determined.

In order to check the results, two different experimental techniques were developed, both of which avoid the dynamic bifurcation effect related to slowly varying bifurcation parameters. While the step measurement (SM) is straightforward, the harmonic burst excitation (HT) needs expensive instrumentation built in the machine tool. The SM technique was strongly influenced by the dynamics of the rotating spindle, which was taken into account by the method presented in [53]. Qualitative agreement was shown between theory and experiments with theoretical results being somewhat shifted compared to the experimental ones. The HT case was presented with less number of measurements, but it can still be considered as an appropriate industrial demonstration of the phenomenon.

In some cases, the SM was not able to capture the phenomenon due to the insufficient resolution of the parameter steps. In the meanwhile, especially in the HT case, noise induced vibrations caused resonance of the nearby multipliers, which can be taken mistakenly as chatter vibration. Still, it is now confirmed even in case of an industrial case study that the presented theory is capable of predicting the qualitative behaviour of milling processes for small and large perturbations, that is, both on linear and nonlinear level. This mostly experimental work proved that subcritical bifurcation, that is, bistability phenomenon exists in milling processes, although it is extremely difficult to obtain accurate quantified agreement between theory and experiments.

The bistable behaviour is experienced by the machinist through the asymmetric behaviour of certain machining operations. These observations are explained the intricate delayed and nonlinear dynamics that originates in the milling process itself. This phenomenon appears already without the consideration of the fly-over effect, which limits the growing nonlinear vibrations. In milling processes, the fly-over appears in strange rhythms due to the multiple edge arrangements, which, in extreme cases can cause even a full one-revolution escape of the tool. Many effects including run-out and rubbing/cutting transitions [76] influence this complex but still pure geometric picture, which all need to be considered for an improved approach. From industrial view-point it would be also useful if those chatter states were selected and characterized, which are still acceptable due to their moderate vibration amplitudes.

8. Acknowledgement

This work was partially supported by European Research Council under the European Unions Seventh Framework Programme (FP7/2007-2013) ERC Advanced grant agreement, No. 340889, Hungarian EMMI ÚNKP Bolyai+ (ÚNKP-18-4-BME-193), Hungarian NKFI FK 124361, EU MC-Suite project (H2020-FoF-2015-680478), EU Marie Skłodowska-Curie IF 704133 Piezomach, NSERC Discovery Accelerator Supplement Grant 477876-2015.

References

1. Tlusty J, Spacek L.
   Self-excited vibrations on machine tools.
   Nakl. CSAV, Prague; 1954.
   In Czech.
2. Tobias S.
   Machine-tool Vibration.
   Blackie, Glasgow; 1965.
3. Hale JK.
   Theory of functional differential equations.
   New York: Springer-Verlag; 1977.
4. Kuljanic E, Totis G, Sortino M.
   Development of an intelligent multisensor chatter detection system in milling.
   Mechanical Systems and Signal Processing. 2009;23(5):1704–1718.
5. Law M, Altintas Y, Srikantha PA.
   Rapid evaluation and optimization of machine tools with position-dependent stability.
   International Journal of Machine Tools & Manufacture. 2013;68(1):81–90.
6. Taner TL, Budak E, Bilgen S, Zatarain M.
   Process simulation integrated tool axis selection for 5-axis tool path generation.
   CIRP Annals - Manufacturing Technology. 2016;65:381–384.
7. Ozturk E, Comak A, Budak E.
   Tuning of tool dynamics for increased stability of parallel (simultaneous) turning processes.
   Journal of Sound and Vibration. 2016;360(1):17–30.
8. Daghini L, Archenti A, Osterlind T.
   Extending stability limits by designed-in damping.
   Journal of Mechanical Engineering. 2013;13(1):37–48.
9. Urbikain G, Campa FJ, Zulaika JJ, Lopez de Lacalle LN, Alonso MA, Collado V.
   Preventing chatter vibrations in heavy-duty turning operations in large horizontal lathes.
   Journal of Sound and Vibration. 2015;340(1):317–330.
10. Li XQ, Wong YS, Nee AYC.
    Tool wear and chatter detection using the coherence function of two crossed accelerations.
    International Journal of Machine Tools and Manufacture. 1997;37(4):425–435.
11. Merritt HE.
    Theory of self-excited machine tool chatter.
    ASME J Eng Ind. 1965;87:447–454.
12. Willis AP, Peixinho J, Kerswell RR, Mullin T.
    Experimental and theoretical progress in pipe flow transition.
    Phil Trans R Soc Lond A. 2008;366:2671–2684.
13. Farkas M.
    Periodic Motions.
    Berlin and New York: Springer-Verlag; 1994.
14. Ince EL.
    Ordinary differential equations.
    London: Longmans, Green and Co.; 1926.
15. van der Pol F, O SMJ.
    On the stability of the solutions of Mathieu's equation.
    Philosophical Magazine and Journal of Science. 1928;5(1):18–38.
16. Minis I, Yanushevsky R.
    A New Theoretical Approach for the Prediction of Machine Tool Chatter in Milling.
    ASME, Journal of Engineering for Industry. 1993;115:1–8.
17. Altintas Y.
    Manufacturing Automation: Metal Cutting Mechanics, Machine Tool Vibrations, and CNC Design.
    Cambridge University Press; 2012.
18. Davies MA, Pratt JR, Dutterer BS, Burns TJ.
    Stability Prediction for Low Radial Immersion Milling.
    Journal of Manufacturing Science and Engineering. 2002;124(2):217–226.

19. Altintas Y, Budak E.
Analytical prediction of stability lobes in milling.
CIRP Annals - Manuf Tech. 1995;44:357–362.
20. Stepan G.
Retarded dynamical systems.
London: Longman; 1989.
21. Budak E, Altintas Y.
Analytical Prediction of Chatter Stability in Milling—Part I: General Formulation.
Journal of Dynamic Systems, Measurement, and Control. 1998;120(1):22–30.
22. Merdol SD, Altintas Y.
Multi Frequency Solution of Chatter Stability for Low Immersion Milling.
Journal of Manufacturing Science and Engineering. 2004;126(3):459–466.
23. Bachrathy D, Stepan G.
Improved prediction of stability lobes with extended multi frequency solution.
CIRP Annals - Manufacturing Technology. 2013;62(1):411–414.
24. Sims ND.
Multi-frequency Chatter Analysis Using the Shift Theorem.
Procedia IUTAM. 2017;22:3–9.
25. Lehotzky D, Insperger T.
A pseudospectral tau approximation for time delay systems and its comparison with other weighted residual type methods.
Int J Numer Meth Eng. 2016;108(6):588–613.
26. Insperger T, Stepan G.
Semi-discretization method for delayed systems.
International Journal for Numerical Methods in Engineering. 2002;55:503–518.
27. Insperger T, Stepan G.
Semi-Discretization for Time-Delay Systems: Stability and Engineering Applications.
New York: Springer; 2011.
28. Insperger T.
Full-discretization and semi-discretization for milling stability prediction: Some comments.
International Journal of Machine Tools and Manufacture. 2010;50(7):658 – 662.
29. Ding Y, Zhu L, Zhang X, Ding H.
A full-discretization method for prediction of milling stability.
International Journal of Machine Tools and Manufacture. 2010;50(5):502–509.
30. Szalai R, Stepan R, Hogan SJ.
Global dynamics of low immersion high-speed milling.
Chaos. 2004;14(4):1069–1077.
31. Munoa J, Dombovari Z, Mancisidor I, Yang Y, Zatarain M.
Interaction Between Multiple Modes in Milling Processes.
Machining Science and Technology. 2013;17(2):165–180.
32. Iglesias A, Munoa J, Ciurana J, Dombovari Z, Stepan G.
Analytical expressions for chatter analysis in milling operations with one dominant mode.
Journal of Sound and Vibration. 2016;375:403–421.
33. Dombovari Z, Stepan G.
On the bistable zone of milling processes.
Phil Trans R Soc A. 2015;373(2051):20140409.
34. Dombovari Z, Barton DAW, Wilson RE, Stepan G.
On the global dynamics of chatter in the orthogonal cuttingmodel.
International Journal of Non-Linear Mechanics. 2010;46:330–338.
35. Guckenheimer J, Holmes P.
Nonlinear Oscillations.
Springer, New York; 1983.
36. Kalmár-Nagy T, Pratt JR, Davies MA, Kennedy MD.
Experimental and analytical investigation of the subcritical instability in metal cutting.
In: Proceedings of DETC'99. Las Vegas, Nevada, USA; 1999. p. 1–7.
37. Kalmár-Nagy T, Stepan G, Moon FC.
Subcritical Hopf bifurcation in the delay equation model for machine tool vibrations.
Nonlinear Dynamics. 2001;26(2):121–142.

rsta.royalsocietypublishing.org Phil. Trans. R. Soc. A 0000000

38. Stepan G, Kalmar-Nagy T.
Nonlinear regenerative machine tool vibrations.
In: Proceedings of ASME Design Engineering Technical Conference. Sacramento, California; 1997. DETC97/VIB-4021.
39. Szalai R, Stepan G.
Period doubling bifurcation and center manifold reduction in a time-periodic and time-delay model of machining.
Journal of Vibration. 2010;16(7-8):1169–1187.
40. Molnar TG, Dombovari Z, Insperger T, Stepan G.
On the analysis of the double Hopf bifurcation in machining processes via centre manifold reduction.
Proc R Soc A. 2017;473(2207):20170502.
41. Wahi P, Chatterjee A.
Regenerative tool chatter near a codimension 2 Hopf point using multiple scales.
Nonlinear Dynamics. 2005;40:323–338.
42. Wahi P, Chatterjee A.
Self-interrupted regenerative metal cutting in turning.
International Journal of Non-Linear Mechanics. 2008;43(2):111 – 123.
43. Szalai R. Knut: a continuation and bifurcation software for delay-differential equations; 2013.
44. Engelborghs K, Luzyanina T, Samaey G.
DDE-BIFTOOL v. 2.00: a Matlab package for bifurcation analysis of delay differential equations.
Department of Computer Science, K.U. Leuven, Leuven, Belgium; 2001. TW330.
45. Dombovari Z, Wilson RE, Stepan G.
Estimates of the bistable region in metal cutting.
Proceedings of the Royal Society A: Mathematical, Physical and Engineering Science. 2008;464(2100):3255–3271.
46. Stepan G, Dombovari Z, Muñoa J.
Identification of cutting force characteristics based on chatter experiments.
CIRP Annals-Manufacturing Technology. 2011;1:113–116.
47. Sieber J, A GB, Neild SA, Wagg DJ, Krauskopf B.
Experimental continuation of periodic orbits through a fold.
Physical Review Letters. 2008;100(24):244101.
48. Bear SM, Erneux T, Rinzel J.
The Slow Passage Through a Hopf Bifurcation: Delay, Memory Effects, and Resonance.
SIAM Journal on Applied Mathematics. 1989;49(1):55–71.
49. Munoa J, Beudaert X, Dombovari Z, Altintas Y, Budak E, Brecher C, et al.
Chatter suppression techniques in metal cutting.
CIRP Annals - Manufacturing Technology. 2016;65(2):785–808.
50. Dombovari Z, Altintas Y, Stepan G.
The effect of serration on mechanics and stability of milling cutters.
International Journal of Machine Tools and Manufacture. 2010;50(6):511 – 520.
51. Dombovari Z, Stepan G.
The Effect on Helix Angle Variation on Milling Stability.
Journal of Manufacturing Science and Engineering. 2012;134(5):051015(1)–051015(6).
52. Wang JJ, Liang SY.
Chip load kinematics in milling with radial cutter runout.
Journal of engineering for industry. 1996;118:111–116.
53. Stepan G, Hajdu D, Iglesias A, Takacs D, Dombovari Z.
Ultimate capability of variable pitch milling cutters.
CIRP Annals. 2018;accepted:1–4.
54. Merdol SD, Altintas Y.
Mechanics and Dynamics of Serrated Cylindrical and Tapered End Mills.
Journal of Manufacturing Science and Engineering. 2004;126(2):317–326.
55. Turner S, Merdol D, Altintas Y, Ridgway K.
Modelling of the stability of variable helix end mills.
International Journal of Machine Tools and Manufacture. 2007;47(9):1410 – 1416.
Selected papers from the 2nd International Conference on High Performance Cutting, 2nd CIRP International Conference on High Performance Cutting.

56. Sims ND, Mann B, Huyanan S.
Analytical prediction of chatter stability for variable pitch and variable helix milling tools.
Journal of Sound and Vibration. 2008;317(3-5):664 – 686.
57. Yusoff AR, Sims ND.
Optimisation of Variable Helix Tool Geometry for Regenerative Chatter Mitigation.
Int J Mach Tools Manuf. 2011;52(2):133–141.
58. Sims ND.
Fast chatter stability prediction for variable helix milling tools.
Journal of Mechanical Engineering Science. 2015;(online).
59. Otto A, Rauh S, Ihlenfeldt S, Radons G.
Stability of milling with non-uniform pitch and variable helix Tools.
The International Journal of Advanced Manufacturing Technology. 2017;89(9–12):2613–2625.
60. Insperger T, Stepan G.
Stability Analysis of Turning With Periodic Spindle Speed Modulation Via Semi-discretization.
Jourdnal of Vibration and Control. 2004;10:1835–1855.
61. Zatarain M, Bediaga I, Muñoa J, Lizarralde R.
Stability of milling processes with continuous spindle speed variation: Analysis in the frequency and time domains, and experimental correlation.
CIRP Annals - Manufacturing Technology. 2008;57(1):379 – 384.
62. Otto A, Radons G.
Application of spindle speed variation for chatter suppression in turning.
CIRP Journal of Manufacturing Science and Technology. 2013;6(2):102–109.
63. Ewins DJ.
Modal Testing: theory, practice, and applications.
Research Studies Press; 2000.
64. Endres WJ, Loo M.
Modeling cutting process nonlinearity for stability analysis - application to tooling selection for valve-seat machining.
In: Proc. of 5th CIRP Workshop, West Lafayette, USA; 2002. .
65. Molnar TG, Dombovari Z, Insperger T, Stepan G.
Bifurcation analysis of nonlinear time-periodic time-delay systems via semidiscretization.
International Journal for Numerical Methods in Engineering. 2018;x(x):1–13.
66. Kuznetsov Y.
Elements of Applied Bifurcation Theory.
Springer, New York; 1998.
67. Molnar TG, Insperger T, Stepan G.
Analytical estimations of limit cycle amplitude for delay-differential equations.
Electron J Qual Theo. 2016;2016(77):1–10.
68. Shi HM, Tobias SA.
Theory of finite-amplitude machine-tool instability.
Int J Mach Tool Manu. 1984;24(1):45–69.
69. Dombovari Z, Munoa J, Kuske R, Stepan G.
Milling stability for slowly varying parameters.
Procedia CIRP. 2018;x(x):1–4.
70. Kiss AK, Hajdu D, Bachrathy D, Stepan G.
Operational stability prediction in milling based on impact tests.
Mechanical Systems and Signal Processing. 2018;103:327–339.
71. Dombovari Z.
Dominant modal decomposition method.
Journal of Sound and Vibration. 2017;392:56–69.
72. Dombovari Z, Zatarain M, Insperger T.
Dominant Vibration Frequencies in Milling Using Semi-discretization Method.
In: 2nd CIRP Conference on Process Machine Interaction (PMI), Vancouver, BC, Canada, on June 10-11; 2010. .
73. Dombovari Z.
Video footage of step measurements: https://youtu.be/bvSWXjymR_4.
Philos T R Soc A. 2019;.

74. Eynian M.
Prediction of vibration frequencies in milling using modified Nyquist method.
CIRP Journal of Manufacturing Science and Technology. 2015;11(1):73–81.
75. Buckwar E, Kuske R, L'Esperance BL, Soo T.
Noise sensitivity in machine tool vibrations.
Int J Bifurcat Chaos. 2006;16:2407–2416.
76. Biro I, Szalay T.
Extension of empirical specific cutting force model for the process of fine chip-removing milling.
Int J Adv Manuf Tech. 2017;88(9):2735–2743.